Available online at www.sciencedirect.com
SCIENCE DIRECT®
Int. J. Electron. Commun. (AEÜ) 59 (2005) 166–176
International Journal AEÜ of Electronics and Communications
www.elsevier.de/aeue

Comparison of bit error rate and convergence of four different iterative receivers for wireless OFDM-CDM

Friedrich Sanzi*

Business Unit Logistics, Leuze electronic GmbH + Co KG, In der Braike 1, D-73277 Owen-Teck, Germany

Received 19 November 2003; received in revised form 12 April 2004

Abstract

In this paper we investigate four different detection methods for Orthogonal Frequency Division Multiplexing Code Division Multiplexing (OFDM-CDM). The first method applies the Maximum A Posteriori (MAP) algorithm. The second and the third method use detection algorithms which are based on the Minimum Mean Squared Error (MMSE) criterion. The second method uses the Soft Symbol Based (SSB)-MMSE algorithm whereas the third receiver applies the Soft Chip Based (SCB)-MMSE algorithm. The fourth detection method uses a hybrid detection scheme which applies the SCB-MMSE and the Soft Interference Cancellation (SIC) detection method. We concatenate each detection method with the outer channel decoder which allows for iterative decoding at the receiver side. This system can be considered as a serially concatenated iterative decoding scheme whereby the inner decoder is replaced by the respective detection method. For the comparison of the four different detection methods the Bit Error Rate as a function of the signal to noise ratio is used as a performance measure. In addition the convergence of the iterative decoding loop is studied with the Extrinsic Information Transfer (EXIT) chart.

Keywords: OFDM; CDM; Iterative decoding; EXIT chart

1. Introduction

For wireless communication systems Orthogonal Frequency Division Multiplexing (OFDM) has received a lot of attention in the recent years. Therefore, OFDM has become an important modulation scheme for several applications, like Digital Audio Broadcasting (DAB), Terrestrial Digital Video Broadcasting (DVB-T) and Wireless LAN (e.g. IEEE 802.11x and HIPERLAN/2). One advantage of OFDM is that it turns a frequency selective channel into a flat fading channel for each sub-carrier. So, the frequency domain equalizer is just a one tap filter for each sub-carrier. To achieve frequency and/or time diversity, OFDM can be combined with Code Division Multiplexing (CDM), where the signal is spread over several sub-carriers and/or several OFDM symbols using othogonal spreading codes, e.g. Walsh codes. This concept was introduced as OFDM-CDM or Multi-Carrier CDM (MC-CDM) by Fazel [1,3], Yee and Linnartz [2], and Fettweis et al. [4]. At the receiver side the orthogonality between the spreading codes is lost, because the subcarriers are affected by different fading coefficients. This effect is enforced by an interleaver [5]. Due to the non-orthogonality of the spreading codes a diversity gain can be obtained at the receiver. Therefore, suitable data detection and decoding technique must be used which increase the complexity of the receiver. However, as analysed in [5] in detail, an OFDM-CDM system benefits from the loss of the orthogonality between the spreading codes compared to a plain OFDM system because iterative decoding can now be applied at the receiver. As a result, an OFDM-CDM system outperforms a plain OFDM system.

* Tel.: +49 7021 573323; fax: +49 7021 573199.
E-mail address: friedrich.sanzi@leuze.de (F. Sanzi).

1434-8411/$ - see front matter © 2004 Elsevier GmbH. All rights reserved.
doi:10.1016/j.aeue.2004.11.006

To exploit the frequency and/or time diversity in an OFDM-CDM system, suitable detection methods have to be chosen [6]. Therefore in this paper, the authors investigate four different detection methods. All these methods enable iterative processing in a serial concatenation with an outer channel decoder in order to exploit the diversity. The first detection method is based on the Maximum A Posteriori (MAP) algorithm proposed in [5]. However, the MAP detection method exhibits immense complexity, which increases exponentially when the spreading factor and/or the symbol alphabet are increased. The second and the third detection method are based on the Minimum Mean Squared Error (MMSE) detection [6,7]. However, the MMSE detection algorithm has to be expanded in order to process arbitrary a priori knowledge which is fed back from the outer channel decoder. This concept of Soft-MMSE was introduced in [8–10] for FIR channel equalization. In our case, the second method uses the Soft Symbol Based (SSB)-MMSE whereas the third method is based on the Soft Chip Based (SCB)-MMSE detection algorithm. The fourth detection method applies a hybrid detection scheme, which uses the SCB-MMSE for the first and the well-known Soft Interference Cancellation (SIC) detection method for the last iteration passes. SIC for OFDM-CDM was proposed in [11,12]. To obtain an overview of the four detection methods they are listed below.

(i) MAP detection method;
(ii) SSB-MMSE detection method;
(iii) SCB-MMSE detection method;
(iv) Hybrid detection scheme applying the SCB-MMSE and the SIC detection method.

In this paper the performance of the four different detection methods is evaluated on the basis of Bit Error Rate (BER) charts. In addition, the convergence is studied with the Extrinsic Information Transfer chart (EXIT chart), recently introduced in [13–15]. The paper is organized as follows: In Section 2 the system model of the transmitter, the channel and the receiver is presented. In Section 3 the four different detection methods are described in detail. The comparison of the performance by computer simulation is presented in Section 4. The BER as a function of the signal to noise ratio E_b/N_0 is used as a performance measure. Also in this section the convergence of the iterative decoding loop is studied with the EXIT chart. Finally, Section 5 concludes the paper.

2. System model

2.1. Transmitter

The block diagram of the transmitter is given in Fig. 1. The bit sequence b_ν is encoded by a convolutional encoder. Its output signal c_μ consists of the coded bits. The outer interleaver outputs the sequence $\tilde{c}_\mu$. M successive coded bits $\tilde{c}_{M\xi}, \tilde{c}_{M\xi+1}, \ldots, \tilde{c}_{M\xi+M-1}$ are grouped to an M-tuple and

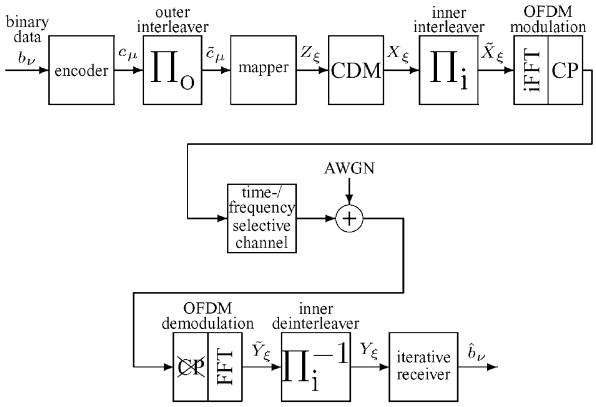

Fig. 1. Transmitter, channel model and receiver for OFDM-CDM.

mapped onto a QAM symbol Z_ξ according to

$$Z_\xi = f_{\text{map},M}(\tilde{c}_{M\xi}, \tilde{c}_{M\xi+1}, \ldots, \tilde{c}_{M\xi+M-1}). \tag{1}$$

We assume, that the outer interleaver and the mapper are designed such that the sequence Z_ξ has zero mean and is uncorrelated. Therefore, the expected value $\mathrm{E}\left\{Z_\xi Z_{\tilde{\xi}}^*\right\}$ is

$$\mathrm{E}\left\{Z_\xi Z_{\tilde{\xi}}^*\right\} = E_S \delta_{\xi-\tilde{\xi}}, \quad \delta_i = \begin{cases} 1 & i = 0, \\ 0 & \text{elsewhere.} \end{cases} \tag{2}$$

$(\cdot)^*$ denotes the conjugate complex operation. Z_ξ is spread by the CDM block which takes N_{CDM} consecutive QAM symbols Z_ξ, creates the vector $\mathbf{u}_{N_{\text{CDM}},m}$ with the components $u_{p,m} = Z_{N_{\text{CDM}}\times m+p}$ ($m \in \mathbb{Z}$ and $p = 0, 1, \ldots, N_{\text{CDM}} - 1$) and multiplies it with the Walsh matrix $\mathbf{W}_{N_{\text{CDM}}}$

$$\mathbf{v}_{N_{\text{CDM}},m}^{\mathrm{T}} = \mathbf{u}_{N_{\text{CDM}},m}^{\mathrm{T}} \mathbf{W}_{N_{\text{CDM}}}. \tag{3}$$

$(\cdot)^{\mathrm{T}}$ denotes the transpose. The resulting vector $\mathbf{v}_{N_{\text{CDM}},m}$ with the elements $v_{q,m}$ is converted to the composite multi-code CDM sequence $X_\xi = v_{\xi \,\text{MOD}\, N_{\text{CDM}},\xi \,\text{DIV}\, N_{\text{CDM}}}$, where MOD is the modulo and DIV is the integer division operator. The set of N_{CDM} orthogonal Walsh-code words can be calculated recursively by using

$$\mathbf{W}_{N_{\text{CDM}}} = \frac{1}{\sqrt{N_{\text{CDM}}}} \begin{pmatrix} \mathbf{W}_{N_{\text{CDM}}/2} & \mathbf{W}_{N_{\text{CDM}}/2} \\ \mathbf{W}_{N_{\text{CDM}}/2} & -\mathbf{W}_{N_{\text{CDM}}/2} \end{pmatrix} \tag{4}$$

with $N_{\text{CDM}} \geqslant 2$, whereby $\mathbf{W}_1 = 1$ and $\mathbf{W}_{N_{\text{CDM}}}$ is the $N_{\text{CDM}} \times N_{\text{CDM}}$ Walsh matrix [16]. N_{CDM} is also called the spreading factor. The elements of $\mathbf{W}_{N_{\text{CDM}}}$ are denoted by $w_{p,q}$ ($p, q = 0, \ldots, N_{\text{CDM}} - 1$) with $w_{p,q} = w_{q,p}$. Therefore, (3) can be expressed as

$$\mathbf{v}_{N_{\text{CDM}},m} = \mathbf{W}_{N_{\text{CDM}}}^{\mathrm{T}} \mathbf{u}_{N_{\text{CDM}},m} = \mathbf{W}_{N_{\text{CDM}}} \mathbf{u}_{N_{\text{CDM}},m}. \tag{5}$$

The serial order of X_ξ is interchanged by the subsequent inner interleaver in Fig. 1 which results in the sequence $\tilde{X}_\xi$. The inner interleaver demolishes the orthogonality of the spreading codes resulting in a better diversity gain [5]. $\tilde{X}_\xi$ is modulated onto K orthogonal sub-carriers by an iFFT-block. Then the guard interval or Cyclic Prefix (CP) is inserted.

The output signal of the OFDM modulator is fed into the time- and frequency-selective channel.

2.2. Channel model

The time varying frequency response of a Wide-Sense Stationary Uncorrelated Scattering (WSSUS) multipath channel can be expressed as [17],

$$H(f,t) = \frac{1}{\sqrt{L}} \sum_{i=1}^{L} \mathrm{e}^{j(\varphi_i + 2\pi f_{\mathrm{D}_i} t - 2\pi f \tau_i)}, \tag{6}$$

where f and t are continuous frequency and time resp., φ_i is the phase, f_{D_i} the Doppler frequency and τ_i the delay of the ith path. L denotes the number of propagation paths. In the following we assume that $H(f,t)$ in (6) is approximately unchanged during the duration T_s of one OFDM symbol. Under this assumption and provided that the guard interval is longer than the delay spread of the channel, the cyclic prefix avoids Inter-Carrier Interference (ICI) as well as Inter-Symbol Interference (ISI). In this case, we obtain the received QAM constellation points $\tilde{Y}_\xi$ in Fig. 1 after the removal of the Cyclic Prefix (CP) and OFDM demodulation with FFT

$$\tilde{Y}_\xi = \tilde{H}_\xi \tilde{X}_\xi + \tilde{N}_\xi, \tag{7}$$

whereby $\tilde{X}_\xi$ are the transmitted signal constellation points and $\tilde{N}_\xi$ are statistically independent and identically distributed complex Gaussian noise variables with component-wise noise power $\sigma^2_{\tilde{N}} = N_0/2$. Therefore, the expected value $\mathrm{E}\left\{\tilde{N}_\xi \tilde{N}^*_{\tilde{\xi}}\right\}$ is

$$\mathrm{E}\left\{\tilde{N}_\xi \tilde{N}^*_{\tilde{\xi}}\right\} = N_0 \delta_{\xi-\tilde{\xi}}. \tag{8}$$

The $\tilde{H}_\xi$ in (7) are sample values of the channel frequency response

$$\tilde{H}_\xi = H((\xi \,\mathrm{MOD}\, K)\Delta f, (\xi \,\mathrm{DIV}\, K)T_\mathrm{s}), \tag{9}$$

whereby Δf is the sub-carrier spacing and T_s is the duration of one OFDM symbol (useful part plus guard interval). After the inner deinterleaver the received QAM constellation points Y_ξ in Fig. 1 can be calculated as

$$Y_\xi = H_\xi X_\xi + N_\xi. \tag{10}$$

In the following we assume that the inner interleaver size is big enough in order to achieve almost perfect time and frequency interleaving. Therefore, H_ξ are modeled as statistically independent and identically distributed complex Gaussian variables with component-wise power $\sigma^2_H = \frac{1}{2}$ and zero mean (see [6]). According to (8), the expected value $\mathrm{E}\left\{H_\xi H^*_{\tilde{\xi}}\right\}$ can be computed as

$$\mathrm{E}\left\{H_\xi H^*_{\tilde{\xi}}\right\} = 1\delta_{\xi-\tilde{\xi}}. \tag{11}$$

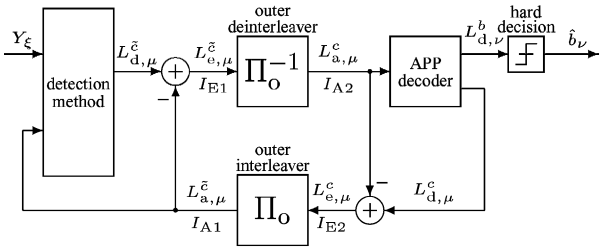

Fig. 2. Iterative receiver.

Due to the inner deinterleaver, the N_ξ in (10) are also statistically independent and identically distributed complex Gaussian noise variables with component-wise noise power $\sigma^2_N = \sigma^2_{\tilde{N}} = N_0/2$ and the expected value $\mathrm{E}\left\{N_\xi N^*_{\tilde{\xi}}\right\}$ is

$$\mathrm{E}\left\{N_\xi N^*_{\tilde{\xi}}\right\} = N_0 \delta_{\xi-\tilde{\xi}}. \tag{12}$$

2.3. Iterative receiver

The signal Y_ξ in Fig. 1 is fed into the iterative receiver which is shown in detail in Fig. 2. The iterative receiver is applied because of the CDM block at the transmitter. The detection method outputs a log-likelihood ratio $L^{\tilde{c}}_{\mathrm{d},\mu}$ (L-value, see [18]) for each coded bit $\tilde{c}_\mu$. After subtracting the a priori knowledge $L^{\tilde{c}}_{\mathrm{a},\mu}$, the L-values $L^{\tilde{c}}_{\mathrm{e},\mu}$ are obtained. They are the input of the outer deinterleaver, which outputs the L-values $L^{c}_{\mathrm{a},\mu}$. They are fed into the APP decoder, which operates according to the soft-in/soft-out principle and computes the A Posteriori Probability (APP or MAP calculator, see [19]). After a hard decision the estimates $\hat{b}_\nu$ of the transmitted bits b_ν are available. This can be accomplished by just taking the sign of the APP decoder output $L^{b}_{\mathrm{d},\nu}$. To allow for turbo processing with iterative detection and decoding, the extrinsic information $L^{c}_{\mathrm{e},\mu}$ of the coded bits c_μ is fed back from the APP decoder, and after the outer interleaving it becomes a priori knowledge $L^{\tilde{c}}_{\mathrm{a},\mu}$ for the detection method and the iteration loop is closed. The four detection methods, which we compare in this paper, will be described in the next section.

3. Alternative detection methods

We are now considering the four alternative detection methods (i)–(iv) more closely.

3.1. MAP detection method

The MAP detection method operates block-wise and takes N_CDM consecutive symbols Y_ξ and $N_\mathrm{ov} = N_\mathrm{CDM} M$ L-values $L^{\tilde{c}}_{\mathrm{a},\mu}$ of the coded bits $\tilde{c}_\mu$. It outputs N_ov L-values $L^{\tilde{c}}_{\mathrm{d},\mu}$ of the coded bits $\tilde{c}_\mu$. To explain the principle, we just consider one block with $\mu = 0, 1, \ldots, N_\mathrm{ov} - 1$ in order to renounce

the DIV and MOD operators in the following. The L-value $L^{\tilde{c}}_{\mathrm{d},\mu}$ of bit $\tilde{c}_\mu$ conditioned on $Y_0, \ldots, Y_{N_{\mathrm{CDM}}-1}$ using Bayes rule can be calculated as follows (see [5]):

$$L^{\tilde{c}}_{\mathrm{d},\mu} = L^{\tilde{c}}_{\mathrm{a},\mu} + \ln \frac{\sum_{i=0}^{2^{N_{\mathrm{ov}}-1}-1} A(i,1)\mathrm{e}^{\sum_{\substack{j=0\\ j\neq\mu}}^{N_{\mathrm{ov}}-1} \tilde{c}_j L^{\tilde{c}}_{\mathrm{a},j}}}{\sum_{i=0}^{2^{N_{\mathrm{ov}}-1}-1} A(i,0)\mathrm{e}^{\sum_{\substack{j=0\\ j\neq\mu}}^{N_{\mathrm{ov}}-1} \tilde{c}_j L^{\tilde{c}}_{\mathrm{a},j}}} \tag{13}$$

with

$$A(i,\tilde{c}_\mu) = p(Y_0, \ldots, Y_{N_{\mathrm{CDM}}-1} | \tilde{c}_\mu, \tilde{c}_{j,j=0,\ldots,N_{\mathrm{ov}}-1, j\neq\mu}). \tag{14}$$

The values of the coded bits $\tilde{c}_j$ in (14) accomplish the following equation:

$$\sum_{j=0}^{\mu-1} \tilde{c}_j 2^j + \sum_{j=\mu+1}^{N_{\mathrm{ov}}-1} \tilde{c}_j 2^{j-1} = i. \tag{15}$$

The a priori L-values can be expressed as

$$L^{\tilde{c}}_{\mathrm{a},\mu} = L_{\mathrm{a}}(\tilde{c}_\mu) = \ln \frac{\Pr[\tilde{c}_\mu = 1]}{\Pr[\tilde{c}_\mu = 0]}, \quad \mu = 0, \ldots, N_{\mathrm{ov}}-1. \tag{16}$$

In order to calculate the probability density function (pdf) $p(\ldots|\ldots)$ in (14) the considered bit sequence has to be mapped and spread according to (1) and (3), which corresponds to the processing at the transmitter in Fig. 1. After this processing, we can derive the L-value $L^{\tilde{c}}_{\mathrm{d},\mu}$ as follows:

$$L^{\tilde{c}}_{\mathrm{d},\mu} = L^{\tilde{c}}_{\mathrm{a},\mu} + \ln \frac{\sum_{i=0,\tilde{c}_\mu=1}^{2^{N_{\mathrm{ov}}-1}-1} C(i,1)\mathrm{e}^{\sum_{\substack{j=0\\ j\neq\mu}}^{N_{\mathrm{ov}}-1} \tilde{c}_j L^{\tilde{c}}_{\mathrm{a},j}}}{\sum_{i=0,\tilde{c}_\mu=0}^{2^{N_{\mathrm{ov}}-1}-1} C(i,0)\mathrm{e}^{\sum_{\substack{j=0\\ j\neq\mu}}^{N_{\mathrm{ov}}-1} \tilde{c}_j L^{\tilde{c}}_{\mathrm{a},j}}} \tag{17}$$

with

$$C(i,\tilde{c}_\mu) = p(Y_0, \ldots, Y_{N_{\mathrm{CDM}}-1} | X_0, \ldots, X_{N_{\mathrm{CDM}}-1}) \tag{18}$$

and

$$(X_0, \ldots, X_{N_{\mathrm{CDM}}-1}) \overset{(3)}{=} (Z_0, \ldots, Z_{N_{\mathrm{CDM}}-1})\mathbf{W}_{N_{\mathrm{CDM}}} \tag{19}$$

and

$$Z_\xi \overset{\tilde{c}_\mu,(15),(1)}{=} f_{\mathrm{map},M}(\tilde{c}_{M\xi}, \tilde{c}_{M\xi+1}, \ldots, \tilde{c}_{M\xi+M-1}). \tag{20}$$

Taking (12) into account, we obtain from (18)

$$C(i,\tilde{c}_\mu) \overset{\tilde{c}_\mu,(15)}{=} \prod_{\xi=0}^{N_{\mathrm{CDM}}-1} p(Y_\xi | X_\xi). \tag{21}$$

According to [5], $p(Y_\xi|X_\xi)$ can be expressed as

$$p(Y_\xi|X_\xi) = \frac{1}{2\pi\sigma_N^2}\mathrm{e}^{-\frac{1}{2\sigma_N^2}|Y_\xi - H_\xi X_\xi|^2}. \tag{22}$$

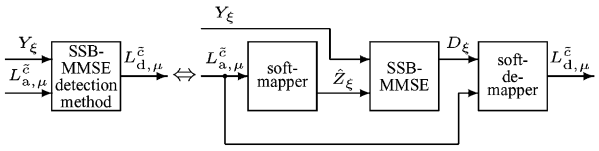

Fig. 3. SSB-MMSE detection method.

Inserting (21) and (22) into (17) results in

$$L^{\tilde{c}}_{\mathrm{d},\mu} = L^{\tilde{c}}_{\mathrm{a},\mu} + \ln \frac{\sum_{i=0,\tilde{c}_\mu=1}^{2^{N_{\mathrm{ov}}-1}-1} \mathrm{e}^{-\frac{\sum_{\xi=0}^{N_{\mathrm{CDM}}-1}|Y_\xi - H_\xi X_\xi|^2}{2\sigma_N^2}} \mathrm{e}^{\sum_{\substack{j=0\\ j\neq\mu}}^{N_{\mathrm{ov}}-1} \tilde{c}_j L^{\tilde{c}}_{\mathrm{a},j}}}{\sum_{i=0,\tilde{c}_\mu=0}^{2^{N_{\mathrm{ov}}-1}-1} \mathrm{e}^{-\frac{\sum_{\xi=0}^{N_{\mathrm{CDM}}-1}|Y_\xi - H_\xi X_\xi|^2}{2\sigma_N^2}} \mathrm{e}^{\sum_{\substack{j=0\\ j\neq\mu}}^{N_{\mathrm{ov}}-1} \tilde{c}_j L^{\tilde{c}}_{\mathrm{a},j}}}. \tag{23}$$

3.2. SSB-MMSE detection method

As depicted in Fig. 3, the SSB-MMSE detection method consists of a soft-mapper, a SSB-MMSE and a soft-demapper. In the following, the building blocks are described in detail.

3.2.1. Soft-mapper

The soft-mapper takes M consecutive a priori L-values $L^{\tilde{c}}_{\mathrm{a},\mu}$ of the coded bits $\tilde{c}_\mu$ at its input in order to calculate the soft-symbol $\hat{Z}_\xi$. Given $L^{\tilde{c}}_{\mathrm{a},\mu}$, we find from (16)

$$\frac{\Pr[\tilde{c}_\mu = 1]}{\Pr[\tilde{c}_\mu = 0]} = \frac{\Pr[\tilde{c}_\mu = 1]}{1 - \Pr[\tilde{c}_\mu = 1]} = \mathrm{e}^{L^{\tilde{c}}_{\mathrm{a},\mu}} \tag{24}$$

and the probabilities $\Pr[\tilde{c}_\mu = 1]$ and $\Pr[\tilde{c}_\mu = 0]$ can be expressed as

$$\Pr[\tilde{c}_\mu = 1] = \frac{1}{2}\left(1 + \tanh\left(\frac{L^{\tilde{c}}_{\mathrm{a},\mu}}{2}\right)\right) \tag{25}$$

and

$$\Pr[\tilde{c}_\mu = 0] = \frac{1}{2}\left(1 - \tanh\left(\frac{L^{\tilde{c}}_{\mathrm{a},\mu}}{2}\right)\right). \tag{26}$$

Using the probabilities $\Pr[\tilde{c}_\mu = 1]$ and $\Pr[\tilde{c}_\mu = 0]$, we can calculate the soft-symbol $\hat{Z}_\xi$ as expected value of Z_ξ

$$\hat{Z}_\xi = \mathrm{E}\{Z_\xi\} = \sum_{i=0}^{2^M-1} B_i f_{\mathrm{map},M}(\tilde{c}_{M\xi+0}, \ldots, \tilde{c}_{M\xi+M-1}), \tag{27}$$

where the factors B_i are given by

$$B_i = \prod_{j=0}^{M-1} \Pr[\tilde{c}_{M\xi+j}] \tag{28}$$

and the values of the coded bits $\tilde{c}_{M\xi+j}$ in (27) and (28) accomplish the equation

$$\sum_{j=0}^{M-1} \tilde{c}_{M\xi+j} 2^j = i. \tag{29}$$

Beyond it, the soft-mapper calculates the variance e_ξ^2 of the soft-symbol $\hat{Z}_\xi$ according to [20].

$$e_\xi^2 = \mathrm{E}\left\{|Z_\xi - \hat{Z}_\xi|^2\right\} = \sum_{i=0}^{2^M-1} B_i \left| f_{\mathrm{map},M}(\ldots) - \hat{Z}_\xi \right|^2. \tag{30}$$

3.2.2. SSB-MMSE

The SSB-MMSE operates block-wise and takes N_{CDM} consecutive received symbols Y_ξ and N_{CDM} consecutive soft-symbols $\hat{Z}_\xi$. It outputs N_{CDM} symbols D_ξ. For the explanation of its operation, we just consider one block with $\xi = 0, 1, \ldots, N_{\mathrm{CDM}} - 1$ in order to renounce the DIV and MOD operator in the following. For a block of N_{CDM} consecutive symbols Y_ξ we can find the following equation:

$$\mathbf{y} = \mathbf{H}\mathbf{W}_{N_{\mathrm{CDM}}}\mathbf{z} + \mathbf{n}, \tag{31}$$

where $\mathbf{y}^{\mathrm{T}} = (Y_0\ Y_1\ \ldots\ Y_{N_{\mathrm{CDM}}-1})$ and the channel matrix $\mathbf{H}$ is a $N_{\mathrm{CDM}} \times N_{\mathrm{CDM}}$ diagonal matrix.

$$\mathbf{H} = \begin{pmatrix} H_0 & 0 & 0 & \cdots & 0 \\ 0 & H_1 & 0 & \ddots & \vdots \\ \vdots & \ddots & \ddots & \ddots & \vdots \\ 0 & \cdots & 0 & H_{N_{\mathrm{CDM}}-2} & 0 \\ 0 & 0 & \cdots & 0 & H_{N_{\mathrm{CDM}}-1} \end{pmatrix}. \tag{32}$$

The symbol vector $\mathbf{z}^{\mathrm{T}} = (Z_0\ Z_1\ \ldots\ Z_{N_{\mathrm{CDM}}-1})$ consists of the symbols $Z_\xi \cdot \mathbf{n}^{\mathrm{T}} = (N_0\ N_1\ \ldots\ N_{N_{\mathrm{CDM}}-1})$ in (31) is the additive noise vector. Combining $\mathbf{W}_{N_{\mathrm{CDM}}}$ and $\mathbf{H}$ in (31) gives

$$\mathbf{y} = \mathbf{V}\mathbf{z} + \mathbf{n} \quad \text{with } \mathbf{V} = \mathbf{H}\mathbf{W}_{N_{\mathrm{CDM}}}. \tag{33}$$

The SSB-MMSE calculates the output symbol

$$D_\xi = \Upsilon(\mathbf{d}_\xi, \xi), \tag{34}$$

whereby the operator $\Upsilon\ (\mathbf{a}, k)$ takes out the kth element of the vector $\mathbf{a}$. According to [8–10], the vector $\mathbf{d}_\xi$ in (34) can be calculated as

$$\mathbf{d}_\xi = \mathrm{E}_\xi\{\mathbf{z}\} + \mathbf{V}_{\mathrm{eq},\xi}(\mathbf{y} - \mathbf{V}\mathrm{E}_\xi\{\mathbf{z}\}), \tag{35}$$

whereby $\mathrm{E}_k\{\mathbf{a}\}$ takes the expected value of the vector components except for component k. The expected value of component k is set to 0 according to [8–10]. Therefore, $\mathrm{E}_\xi\{\mathbf{z}\}$ can be expressed as

$$\mathrm{E}_\xi\{\mathbf{z}\}^{\mathrm{T}} = \left(\hat{Z}_0, \ldots, \hat{Z}_{\xi-1}, 0, \hat{Z}_{\xi+1}, \ldots, \hat{Z}_{N_{\mathrm{CDM}}-1}\right)^{\mathrm{T}}. \tag{36}$$

According to [8–10], the matrix $\mathbf{V}_{\mathrm{eq},\xi}$ in (35) yields to

$$\mathbf{V}_{\mathrm{eq},\xi} = \mathbf{Q}_\xi \mathbf{V}^{\mathrm{H}} (\mathbf{V}\mathbf{Q}_\xi \mathbf{V}^{\mathrm{H}} + N_0 \mathbf{I})^{-1}, \tag{37}$$

whereby $(\cdot)^{\mathrm{H}}$ denotes the conjugate transpose operation and $\mathbf{I}$ is the identity matrix. $\mathbf{Q}_\xi$ is a $N_{\mathrm{CDM}} \times N_{\mathrm{CDM}}$ diagonal matrix with elements $q_{k,k}$. Taking (30) into account, these elements are given by

$$q_{k,k} = \begin{cases} E_{\mathrm{S}} & \text{for } k = \xi, \\ e_k^2 & \text{elsewhere.} \end{cases} \tag{38}$$

The vector $\mathbf{d}_\xi$ in (35) can be expressed as

$$\mathbf{d}_\xi = \mathrm{E}_\xi\{\mathbf{z}\} + \mathbf{G}_\xi(\mathbf{z} - \mathrm{E}_\xi\{\mathbf{z}\}) + \mathbf{V}_{\mathrm{eq},\xi}\mathbf{n} \tag{39}$$

with

$$\mathbf{G}_\xi = \mathbf{V}_{\mathrm{eq},\xi}\mathbf{V}. \tag{40}$$

Using (34), the symbol D_ξ is given by

$$D_\xi = g_{\xi,\xi} Z_\xi + \sum_{\substack{k=0 \\ k\neq\xi}}^{N_{\mathrm{CDM}}-1} g_{\xi,k}(Z_k - \hat{Z}_k) + \sum_{k=0}^{N_{\mathrm{CDM}}-1} v_{\mathrm{eq},\xi,k} N_k. \tag{41}$$

The elements of matrix $\mathbf{G}_\xi$ are denoted by $g_{m,k}$ and the elements of matrix $\mathbf{V}_{\mathrm{eq},\xi}$ by $v_{\mathrm{eq},m,k}$. Combining all interference terms, (41) becomes

$$D_\xi = G_\xi Z_\xi + \hat{N}_\xi \quad \text{with } G_\xi = g_{\xi,\xi} \tag{42}$$

and

$$\hat{N}_\xi = \sum_{\substack{k=0 \\ k\neq\xi}}^{N_{\mathrm{CDM}}-1} g_{\xi,k}(Z_k - \hat{Z}_k) + \sum_{k=0}^{N_{\mathrm{CDM}}-1} v_{\mathrm{eq},\xi,k} N_k. \tag{43}$$

According to [6], $\hat{N}_\xi$ can be considered as additive zero-mean Gaussian noise with noise power $2\sigma_{\hat{N}_\xi}^2 = \mathrm{E}\{\hat{N}_\xi \hat{N}_\xi^*\}$ which can be expressed as

$$2\sigma_{\hat{N}_\xi}^2 = \sum_{\substack{k=0 \\ k\neq\xi}}^{N_{\mathrm{CDM}}-1} |g_{\xi,k}|^2 e_k^2 + N_0 \sum_{k=0}^{N_{\mathrm{CDM}}-1} |v_{\mathrm{eq},\xi,k}|^2. \tag{44}$$

3.2.3. Soft-demapper

The soft-demapper outputs M L-values $L_{\mathrm{d},\mu}^{\tilde{c}}$ of the coded bits $\tilde{c}_\mu$ for each symbol D_ξ. For explanation, we regard only one symbol D_0, G_0 and $\mu = 0, \ldots, M-1$ in the following. As a consequence, we calculate the L-values $L_{\mathrm{d},\mu}^{\tilde{c}}$ of the symbol Z_0. According to [21,22], the L-value $L_{\mathrm{d},\mu}^{\tilde{c}}$ of bit $\tilde{c}_\mu$ conditioned on D_0 using Bayes rule can be calculated as

$$L_{\mathrm{d},\mu}^{\tilde{c}} = L_{\mathrm{a},\mu}^{\tilde{c}} + \ln \frac{\sum_{i=0}^{2^{M-1}-1} F(i,1) \mathrm{e}^{\sum_{\substack{j=0 \\ j\neq\mu}}^{M-1} \tilde{c}_j L_{\mathrm{a},j}^{\tilde{c}}}}{\sum_{i=0}^{2^{M-1}-1} F(i,0) \mathrm{e}^{\sum_{\substack{j=0 \\ j\neq\mu}}^{M-1} \tilde{c}_j L_{\mathrm{a},j}^{\tilde{c}}}} \tag{45}$$

with

$$F(i,\tilde{c}_\mu) = p(D_0|\tilde{c}_\mu, \tilde{c}_{j,j=0,\ldots,M-1,j\neq\mu}). \tag{46}$$

The values of the coded bits $\tilde{c}_j$ in (45) accomplish the following equation:

$$\sum_{j=0}^{\mu-1} \tilde{c}_j 2^j + \sum_{j=\mu+1}^{M-1} \tilde{c}_j 2^{j-1} = i. \tag{47}$$

The pdf $p(D_0|\tilde{c}_\mu, \tilde{c}_{j,j=0,\ldots,M-1,j\neq\mu})$ in (46) can be expressed as (see [21,22])

$$p(D_0|\tilde{c}_\mu, \tilde{c}_j) \overset{(42),(44)}{=} \frac{1}{2\pi\sigma^2_{\hat{N}_0}} \mathrm{e}^{-\frac{1}{2\sigma^2_{\hat{N}_0}}|D_0 - G_0 f_{\mathrm{map},M}(\tilde{c}_\mu,\tilde{c}_j)|^2}. \tag{48}$$

Inserting (46) and (48) into (45) results in

$$L^{\tilde{c}}_{\mathrm{d},\mu} = L^{\tilde{c}}_{\mathrm{a},\mu} + \ln \frac{\sum_{i=0,\tilde{c}_\mu=1}^{2^{M-1}-1} \mathrm{e}^{-\frac{1}{2\sigma^2_{\hat{N}_0}}|D_0 - G_0 f_{\mathrm{map},M}(\tilde{c}_\mu,\tilde{c}_j)|^2} \mathrm{e}^{\sum_{j=0,j\neq\mu}^{M-1} \tilde{c}_j L^{\tilde{c}}_{\mathrm{a},j}}}{\sum_{i=0,\tilde{c}_\mu=0}^{2^{M-1}-1} \mathrm{e}^{-\frac{1}{2\sigma^2_{\hat{N}_0}}|D_0 - G_0 f_{\mathrm{map},M}(\tilde{c}_\mu,\tilde{c}_j)|^2} \mathrm{e}^{\sum_{j=0,j\neq\mu}^{M-1} \tilde{c}_j L^{\tilde{c}}_{\mathrm{a},j}}}. \tag{49}$$

3.3. SCB-MMSE detection method

The structure of this method is almost identical to the block diagram depicted in Fig. 3, except the SSB-MMSE which has to be replaced by the SCB-MMSE. Therefore, only the SCB-MMSE is described in detail in the following.

3.3.1. SCB-MMSE

The SCB-MMSE operates block-wise and takes N_{CDM} consecutive symbols Y_ξ and outputs N_{CDM} symbols D_ξ. For the explanation we just consider one block with $\xi = 0, 1, \ldots, N_{\mathrm{CDM}} - 1$ in order to renounce the DIV and MOD operator in the following. The first step in the determination of D_ξ is the calculation of the symbol S_k as follows:

$$S_k = \mathrm{E}\{X_k\} + H_{\mathrm{eq},k}(Y_k - H_k \mathrm{E}\{X_k\}), \tag{50}$$

$$S_k = \mathrm{E}\{X_k\} + H_{\mathrm{eq},k} H_k (X_k - \mathrm{E}\{X_k\}) + H_{\mathrm{eq},k} N_k. \tag{51}$$

Using (3) and (4), $\mathrm{E}\{X_k\}$ with $k = 0, \ldots, N_{\mathrm{CDM}} - 1$ can be expressed as

$$\mathrm{E}\{X_k\} = \sum_{p=0}^{N_{\mathrm{CDM}}-1} \mathrm{E}_\xi\{Z_p\} w_{p,k} \tag{52}$$

with

$$\mathrm{E}_\xi\{Z_p\} \overset{(27)}{=} \begin{cases} 0 & \text{for } p = \xi, \\ \hat{Z}_p & \text{elsewhere.} \end{cases} \tag{53}$$

$H_{\mathrm{eq},k}$ in (50) can be computed according to (37) as

$$H_{\mathrm{eq},k} = Q_k H_k^{\mathrm{H}} (H_k Q_k \cdot H_k^{\mathrm{H}} + N_0)^{-1} \tag{54}$$

with

$$Q_k = \mathrm{E}\left\{|X_k - \mathrm{E}\{X_k\}|^2\right\} \tag{55}$$

and

$$Q_k \overset{(3),(4)}{=} \mathrm{E}\left\{\left|\sum_{p=0}^{N_{\mathrm{CDM}}-1} (Z_p - \mathrm{E}_\xi\{Z_p\}) w_{p,k}\right|^2\right\}, \tag{56}$$

$$Q_k \overset{(2)}{=} \sum_{p=0}^{N_{\mathrm{CDM}}-1} \mathrm{E}\left\{|Z_p - \mathrm{E}_\xi\{Z_p\}|^2\right\} |w_{p,k}|^2. \tag{57}$$

Taking (30) into account, we get

$$\mathrm{E}\{|Z_p - \mathrm{E}_\xi\{Z_p\}|^2\} = \begin{cases} E_{\mathrm{S}} & \text{for } p = \xi, \\ e_p^2 & \text{elsewhere.} \end{cases} \tag{58}$$

Using (58), Q_k in (57) can be calculated.

Rewriting (50), we obtain

$$S_k = \mathrm{E}\{X_k\} + V_k(X_k - \mathrm{E}\{X_k\}) + H_{\mathrm{eq},k} N_k \tag{59}$$

with

$$V_k = H_{\mathrm{eq},k} H_k. \tag{60}$$

Taking (3) and (4) into account, (59) results in

$$S_k = \sum_{p=0}^{N_{\mathrm{CDM}}-1} \mathrm{E}_\xi\{Z_p\} w_{p,k} + V_k \sum_{p=0}^{N_{\mathrm{CDM}}-1} (Z_p - \mathrm{E}_\xi\{Z_p\}) w_{p,k} + H_{\mathrm{eq},k} N_k. \tag{61}$$

After the calculation of S_k, the inverse CDM operation follows in the second step. For that purpose, N_{CDM} symbols S_k are put together in order to form the vector $\mathbf{s}_\xi$

$$\mathbf{s}_\chi^{\mathrm{T}} = (S_0, \ldots, S_{N_{\mathrm{CDM}}-1}). \tag{62}$$

Then $\mathbf{s}_\chi$ is multiplied by the Walsh matrix $\mathbf{W}_{N_{\mathrm{CDM}}}$. The result is the vector

$$\mathbf{d}_\chi^{\mathrm{T}} = \mathbf{s}_\chi^{\mathrm{T}} \mathbf{W}_{N_{\mathrm{CDM}}}^{\mathrm{T}} = \mathbf{s}_\chi^{\mathrm{T}} \mathbf{W}_{N_{\mathrm{CDM}}}. \tag{63}$$

The component D_ξ of the vector $\mathbf{d}_\chi$ can be calculated as

$$D_\xi = \sum_{\tilde{p}=0}^{N_{\mathrm{CDM}}-1} S_{\tilde{p}} w_{\xi,\tilde{p}} = \sum_{\tilde{p}=0}^{N_{\mathrm{CDM}}-1} S_{\tilde{p}} w_{\tilde{p},\xi}. \tag{64}$$

By inserting (61) into (64), D_ξ can be expressed as

$$D_\xi = Z_\xi g_{\xi,\xi} + \sum_{\substack{p=0 \\ p\neq\xi}}^{N_{\mathrm{CDM}}-1} (Z_p - \mathrm{E}_\xi\{Z_p\}) g_{\xi,p} + \sum_{\tilde{p}=0}^{N_{\mathrm{CDM}}-1} H_{\mathrm{eq},\tilde{p}} N_{\tilde{p}} w_{\xi,\tilde{p}} \tag{65}$$

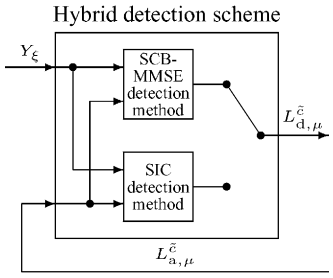

Fig. 4. Hybrid detection scheme.

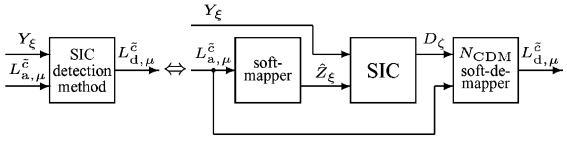

Fig. 5. SIC detection method.

with

$$g_{\xi,p} = \sum_{\tilde{p}=0}^{N_{\mathrm{CDM}}-1} V_{\tilde{p}} w_{p,\tilde{p}} w_{\xi,\tilde{p}}. \tag{66}$$

Combining all interference terms, (65) becomes

$$D_\xi = G_\xi Z_\xi + \hat{N}_\xi \quad \text{with } G_\xi = g_{\xi,\xi} \tag{67}$$

and

$$\hat{N}_\xi = \sum_{\substack{p=0 \\ p\neq\xi}}^{N_{\mathrm{CDM}}-1} (Z_p - \mathrm{E}_\xi\{Z_p\}) g_{\xi,p} + \sum_{\tilde{p}=0}^{N_{\mathrm{CDM}}-1} H_{\mathrm{eq},\tilde{p}} N_{\tilde{p}} w_{\xi,\tilde{p}}. \tag{68}$$

According to [6], $\hat{N}_\xi$ can be considered as additive zero-mean Gaussian noise with noise power $2\sigma^2_{\hat{N}_\xi} = \mathrm{E}\{\hat{N}_\xi \hat{N}^*_\xi\}$ which is

$$2\sigma^2_{\hat{N}_\xi} = \sum_{\substack{p=0 \\ p\neq\xi}}^{N_{\mathrm{CDM}}-1} e_p^2 |g_{\xi,p}|^2 + N_0 \sum_{\tilde{p}=0}^{N_{\mathrm{CDM}}-1} |H_{\mathrm{eq},\tilde{p}} w_{\xi,\tilde{p}}|^2. \tag{69}$$

3.4. Hybrid detection scheme

The structure of the hybrid detection scheme is depicted in Fig. 4 and consists of the SCB-MMSE and the SIC detection method. This hybrid scheme uses the SCB-MMSE for the first iterations and the SIC detection method for the last iterations. Because the SCB-MMSE detection method was already described in Section 3.3, we restrict ourselves to the SIC detection method in the following. The structure of this method is depicted in Fig. 5 and consists of a soft-mapper, a SIC and a N_{CDM} soft-demapper. In the following the SIC and the N_{CDM} soft-demapper are described in detail. The soft-mapper was already explained in Section 3.2.1.

3.4.1. SIC

The SIC operates blockwise. It takes N_{CDM} consecutive symbols Y_ξ and N_{CDM} consecutive soft-symbols $\hat{Z}_\xi$. The SIC outputs $N_{\mathrm{CDM}} N_{\mathrm{CDM}}$ symbols D_ζ. For the explanation, we just regard $\zeta = 0, \ldots, N_{\mathrm{CDM}} N_{\mathrm{CDM}} - 1$ in the following. Taking (3), (4) and (10) into account, the symbol Y_ξ can be calculated as

$$Y_{\tilde{\xi}} = H_{\tilde{\xi}} \sum_{p=0}^{N_{\mathrm{CDM}}-1} Z_p w_{p,\tilde{\xi}} + N_{\tilde{\xi}}, \quad \tilde{\xi} = 0, \ldots, N_{\mathrm{CDM}} - 1. \tag{70}$$

The SIC for symbol Z_ξ calculates the signal $V_{\xi,\tilde{\xi}}$ by subtracting the soft-symbols $\hat{Z}_{\tilde{\xi}}$ of the remaining symbols from $Y_{\tilde{\xi}}$.

$$V_{\xi,\tilde{\xi}} = Y_{\tilde{\xi}} - H_{\tilde{\xi}} \sum_{\substack{p=0 \\ p\neq\xi}}^{N_{\mathrm{CDM}}-1} \hat{Z}_p w_{p,\tilde{\xi}}. \tag{71}$$

Using (70), $V_{\xi,\tilde{\xi}}$ yields to

$$V_{\xi,\tilde{\xi}} = H_{\tilde{\xi}} Z_\xi w_{\xi,\tilde{\xi}} + N_{\xi,\tilde{\xi}}, \qquad \tilde{\xi} = 0, \ldots, N_{\mathrm{CDM}} - 1 \tag{72}$$

with

$$N_{\xi,\tilde{\xi}} = H_{\tilde{\xi}} \sum_{\substack{p=0 \\ p\neq\xi}}^{N_{\mathrm{CDM}}-1} (Z_p - \hat{Z}_p) w_{p,\tilde{\xi}} + N_{\tilde{\xi}}. \tag{73}$$

Under the assumption of zero-mean Gaussian noise $N_{\xi,\tilde{\xi}}$ [6,20], the variance $2\sigma^2_{N_{\xi,\tilde{\xi}}}$ of $N_{\xi,\tilde{\xi}}$ can be computed using (30) as

$$2\sigma^2_{N_{\xi,\tilde{\xi}}} = |H_{\tilde{\xi}}|^2 \sum_{\substack{p=0 \\ p\neq\xi}}^{N_{\mathrm{CDM}}-1} e_p^2 w^2_{p,\tilde{\xi}} + N_0. \tag{74}$$

The output symbol D_ζ of the SIC results in

$$D_\zeta = V_{\xi,\tilde{\xi}}, \qquad \zeta = \tilde{\xi} + \xi N_{\mathrm{CDM}}. \tag{75}$$

3.4.2. N_{CDM} soft-demapper

The N_{CDM} soft-demapper outputs M L-values $L^{\tilde{c}}_{\mathrm{d},\mu}$ of the coded bits $\tilde{c}_\mu$ for N_{CDM} consecutive symbols D_ζ. For the explanation, we regard only the first N_{CDM} symbols $D_0, \ldots, D_{N_{\mathrm{CDM}}-1}$ and $\mu = 0, \ldots, M-1$ in the following. As a consequence of this simplification, we calculate the L-values $L^{\tilde{c}}_{\mathrm{d},\mu}$ of the symbol Z_0. According to (13) and (45), the L-value $L^{\tilde{c}}_{\mathrm{d},\mu}$ of bit $\tilde{c}_\mu$ conditioned on $D_0, \ldots, D_{N_{\mathrm{CDM}}-1}$

using Bayes rule can be calculated as

$$L_{\mathrm{d},\mu}^{\tilde{c}} = L_{\mathrm{a},\mu}^{\tilde{c}} + \ln \frac{\sum_{i=0}^{2^{M-1}-1} L(i,1)\mathrm{e}^{\sum_{j=0,j\neq\mu}^{M-1}\tilde{c}_j\cdot L_{\mathrm{a},j}^{\tilde{c}}}}{\sum_{i=0}^{2^{M-1}-1} L(i,0)\mathrm{e}^{\sum_{j=0,j\neq\mu}^{M-1}\tilde{c}_j\cdot L_{\mathrm{a},j}^{\tilde{c}}}} \tag{76}$$

with

$$L(i,\tilde{c}_\mu) = p(D_0,\ldots,D_{N_{\mathrm{CDM}}-1}|\tilde{c}_\mu,\tilde{c}_{j,j=0,\ldots,M-1,j\neq\mu}). \tag{77}$$

The values of the coded bits $\tilde{c}_j$ in (76) accomplish the following equation:

$$\sum_{j=0}^{\mu-1}\tilde{c}_j 2^j + \sum_{j=\mu+1}^{M-1}\tilde{c}_j 2^{j-1} = i. \tag{78}$$

The pdf $p(D_0,\ldots,D_{N_{\mathrm{CDM}}-1}|\tilde{c}_\mu,\tilde{c}_j)$ in (77) can be expressed as

$$p(D_0,\ldots,D_{N_{\mathrm{CDM}}-1}|\tilde{c}_\mu,\tilde{c}_j) = \prod_{\zeta=0}^{N_{\mathrm{CDM}}-1} p(D_\zeta|\tilde{c}_\mu,\tilde{c}_j), \tag{79}$$

whereby

$$p(D_\zeta|\tilde{c}_\mu,\tilde{c}_j) \overset{(72)}{=} \frac{1}{2\pi\sigma_{0,\zeta}^2}\,\mathrm{e}^{-\frac{1}{2\sigma_{N_{0,\zeta}}^2}|V_{0,\zeta}-H_\zeta f_{\mathrm{map},M}(\tilde{c}_\mu,\tilde{c}_j)w_{0,\zeta}|^2}. \tag{80}$$

Inserting (79) and (80) into (76) results in

$$L_{\mathrm{d},\mu}^{\tilde{c}} = L_{\mathrm{a},\mu}^{\tilde{c}} + \ln \frac{\sum_{i=0,\tilde{c}_\mu=1}^{2^{M-1}-1}\left(\prod_{\zeta=0}^{N_{\mathrm{CDM}}-1}\mathrm{e}^{-\frac{1}{2\sigma_{N_{0,\zeta}}^2}|V_{0,\zeta}-H_\zeta f_{\mathrm{map},M}(\ldots)w_{0,\zeta}|^2}\right)\mathrm{e}^{\sum_{j=0,j\neq\mu}^{M-1}\tilde{c}_j L_{\mathrm{a},j}^{\tilde{c}}}}{\sum_{i=0,\tilde{c}_\mu=0}^{2^{M-1}-1}\left(\prod_{\zeta=0}^{N_{\mathrm{CDM}}-1}\mathrm{e}^{-\frac{1}{2\sigma_{N_{0,\zeta}}^2}|V_{0,\zeta}-H_\zeta f_{\mathrm{map},M}(\ldots)w_{0,\zeta}|^2}\right)\mathrm{e}^{\sum_{j=0,j\neq\mu}^{M-1}\tilde{c}_j L_{\mathrm{a},j}^{\tilde{c}}}}. \tag{81}$$

4. Comparison of the four iterative receivers by simulation

For the calculation of E_b/N_0 we use the following definition:

$$\left.\frac{E_\mathrm{b}}{N_0}\right|_{\mathrm{dB}} = \left.\frac{E_\mathrm{S}}{N_0}\right|_{\mathrm{dB}} + 10\ \mathrm{lg}\ \frac{1}{R_\mathrm{g}R_\mathrm{c}M}, \tag{82}$$

where R_c is the code rate of the encoder and R_g takes the redundancy into account, which is added by the guard interval [23]. As an example, we use $R_\mathrm{g} = 0.8$. Therefore, the duration of the guard interval is considered to be one-fifth of the OFDM symbol duration T_s. As an example, the used convolutional code is recursive systematic with feedback polynomial $G_r = 037$ (octal notation), feedforward polynomial $G = 023$, memory 4 and code rate $R_\mathrm{c} = 0.5$. The outer code does not need to be recursive. The outer interleaver size is $I_{\mathrm{L,out}} = 98,304$. The spreading factor N_{CDM} is set to $N_{\mathrm{CDM}} = 8$ according to [6]. The number M of bits per QAM symbol can vary between 1 (BPSK), 2 (QPSK) and 4 (16-QAM). We further assume, that the channel state information H_ξ is perfectly known at the receiver. Channel estimation for an OFDM–CDM system can be accomplished by inserting pilot symbols into the transmitted data stream (see [23–27]).

Table 1. Complexity of the four different detection methods

	MAP	SSB-MMSE	SCB-MMSE	SIC
BPSK	27.04	27.0	1.0	1.08
QPSK	—	22.22	1.0	1.5
16-QAM	—	10.35	1.0	3.0

4.1. Complexity

In Table 1 the complexity of the different detection methods is compared. The complexity of the hybrid detection scheme (3.4) can be easily derived by proportional linear superposition of the SCB-MMSE and the SIC detection method taking the number of iterations into account. As a measure of complexity simulation time duration is taken. The amount of memory is disregarded. The lowest complexity (shortest simulation time duration) is set to 1.0 for each regarded modulation scheme. So, comparisons in Table 1 should only be done on horizontal lines. As can be seen from Table 1 the SCB-MMSE detection method has the lowest complexity followed by the SIC detection method. However, for 16-QAM the complexity of the SIC detection method is three times higher than the complexity of the SCB-MMSE. The hybrid detection scheme uses the SCB-MMSE and the SIC detection method. Therefore, it combines the two detection methods with low complexity. The complexity of the MAP detection method is only measured for BPSK because of its immense complexity for QPSK and 16-QAM.

4.2. Convergence properties with EXIT chart

Fig. 6 (left) shows the mutual information transfer characteristics of the various detection methods for BPSK and Fig. 6 (right) for 16-QAM with Gray-mapping. The mutual information transfer characteristics are measured for one block of size $I_{\mathrm{L,out}}$ coded bits. The a priori input $L_{\mathrm{a},\mu}^{\tilde{c}}$ to the detection methods is on the abscissa (mutual information $0 \leqslant I_{\mathrm{A1}} \leqslant 1$ in bit per binary symbol). The a posteriori output $L_{\mathrm{e},\mu}^{\tilde{c}}$ is on the ordinate (mutual information $0 \leqslant I_{\mathrm{E1}} \leqslant 1$). I_{A1} and I_{E1} are depicted in Fig. 2 for better understanding. The mutual information transfer characteristics describe the input/output relations of the detection methods and are calculated by applying a Gaussian distributed random variables

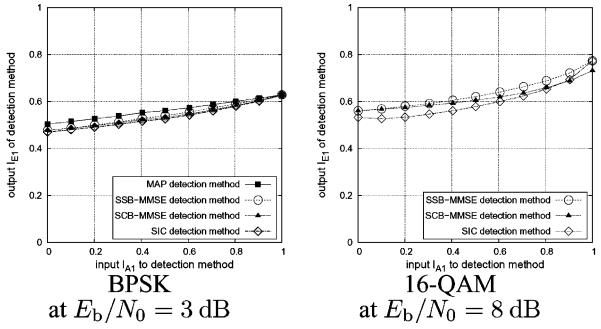

Fig. 6. Mutual information transfer characteristics of the different detection methods for BPSK and 16-QAM.

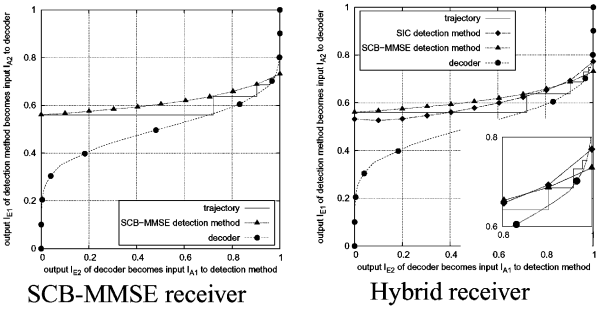

Fig. 7. EXIT chart for SCB-MMSE detection method and hybrid detection scheme (using SCB-MMSE and SIC detection method) and decoder for 16-QAM at $E_b/N_0 = 8$ dB.

as a priori input and quantifying the a posteriori output in terms of mutual information [13–15]. As can be seen, the highest output I_{E1} can be achieved by the MAP detection method. However, for perfect a priori knowledge ($I_{A1} = 1$) the output I_{E1} of the SIC and the SSB-MMSE detection method are identical to the output I_{E1} of the MAP detection method. As a consequence, the performance of the hybrid detection scheme (with SIC for the last iteration passes) or the SSB-MMSE detection method can come close to the receiver with MAP detection method using the iterative decoding loop. The output I_{E1} of the SCB-MMSE detection method is a little bit lower than the others for perfect a priori knowledge. However, the SCB-MMSE detection method is the best in terms of complexity (see Section 4.1). Therefore, the hybrid detection scheme is a compromise between complexity and performance.

In Fig. 7 the EXIT charts are depicted for the receiver with the SCB-MMSE detection method (SCB-MMSE receiver) and the receiver with the hybrid detection scheme (hybrid receiver) for 16-QAM at $E_b/N_0 = 8$ dB. The trajectory (stair case function) is a simulation result of the iterative scheme, whereas the transfer characteristics are computed individually for the detection methods (see Fig. 6) and the decoder, applying Gaussian distributed random variables as a priori inputs. The number of steps in the trajectory is equivalent to the number of iterations. The input $L^c_{a,\mu}$ to the decoder forms the mutual information I_{A2}. The a posteriori output $L^c_{e,\mu}$ of the decoder composes the mutual information I_{E2} (see Fig. 2). The achieved trajectories match fairly well with the transfer characteristics. In case of the SCB-MMSE receiver, the trajectory gets stuck (Fig. 7, left) after 4 iterations, owing to the intersection of the characteristic of SCB-MMSE detection method and the decoder. For the hybrid receiver we pass through the SCB-MMSE detection method three times and use the SIC detection method for the final two passes (3rd and 4th iteration). As can be seen in Fig. 7 (right), the trajectory matches fairly well with the SCB-MMSE detection method characteristic for the first three passes. After that, for the final two passes, it fits with the SIC detection method characteristic (Fig. 7, right, small). The hybrid receiver provides a higher output I_{E1} after the final iteration than the SCB-MMSE receiver. Therefore, the hybrid receiver shows better performance than the SCB-MMSE receiver using the iterative decoding loop.

In Fig. 8 the BER charts of the four different receivers are depicted after various iterations. The number of bits per QAM symbol M is set to 1 for BPSK. For the hybrid receiver the SCB-MMSE detection method is used for the 0th and first iteration. After the first iteration, the SIC detection method is applied. We can conclude from Fig. 8, that the performances of the SSB-MMSE, the hybrid and the SCB-MMSE receiver come close to the performance of the MAP receiver using the iterative decoding loop. After 3 iterations, the curves of the four receivers differ only slightly at a BER lower than 10^{-3}.

In Fig. 9 the BER charts of the SSB-MMSE, the SCB-MMSE and the hybrid receiver are shown after various iterations for 16-QAM. For the hybrid receiver the SCB-MMSE detection method is used for the 0th, first and second iteration. Then, the SIC detection method is applied for the third and 4th iteration. As can be seen in Fig. 9, the performance of the hybrid receiver comes close to the performance of the SSB-MMSE receiver using the iterative decoding loop. After 4 iterations, the curves of the hybrid receiver and SSB-MMSE receiver differ only in a very small E_b/N_0 gap for a BER lower than 10^{-4}. However, the complexity of the hybrid receiver is lower than the complexity of the SSB-MMSE receiver. In comparison to the SCB-MMSE receiver, the hybrid receiver and SSB-MMSE receiver achieve a gain of about $E_b/N_0 = 0.9$ dB at BER 10^{-4} after 4 iterations. Therefore, under the consideration of complexity and performance the hybrid receiver is superior to the other two receivers.

5. Conclusion

We have investigated in quite some detail four different detection methods for a OFDM-CDM system:

(i) MAP detection method;
(ii) SSB-MMSE detection method;
(iii) SCB-MMSE detection method;
(iv) Hybrid detection scheme applying the SCB-MMSE and the SIC detection method.

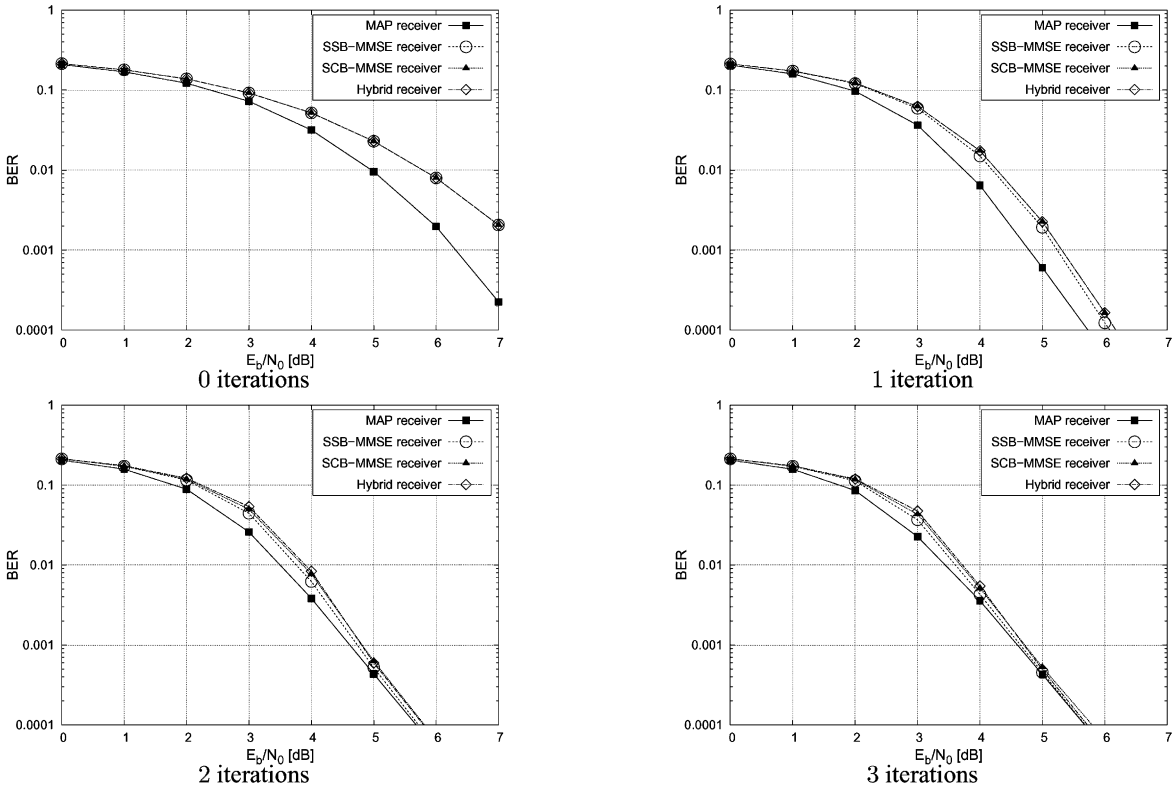

Fig. 8. BER chart of the four different receivers for BPSK after various iterations.

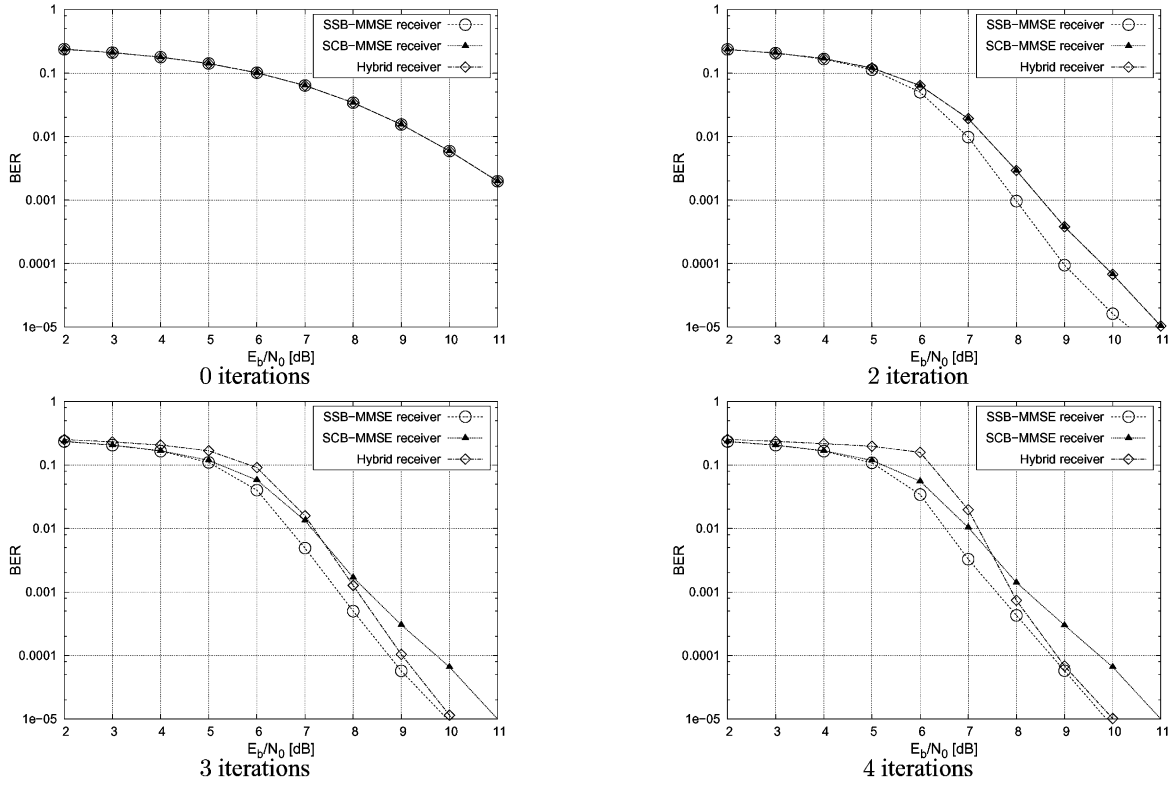

Fig. 9. BER chart of the SSB-MMSE, the SCB-MMSE and the hybrid receiver for 16-QAM after various iterations.

Each detection method is embedded in an iterative detection and decoding loop with an outer channel decoder. It has been shown, that for BPSK the four different receivers achieve nearly the same performance although their complexity is quite different. The MAP receiver is the most complex. Therefore, it was only investigated for BPSK. In the case of 16-QAM the performance of the hybrid and the SSB-MMSE receiver differ only very slightly. In terms of BER these two receivers outperform the SCB-MMSE receiver by about $E_b/N_0 = 0.9\,\text{dB}$ at BER 10^{-4} after 4 iterations. However, the SCB-MMSE receiver has the lowest complexity of all. Therefore, the hybrid receiver is a good compromise between complexity and performance and is therefore recommended.

References

[1] Fazel K. Performance of CDMA/OFDM for mobile communication system. IEEE International Conference on Universal Personal Communications (ICUPC), 1993.

[2] Yee N, Linnartz J-P. BER of multi-carrier CDMA in an indoor rician fading channel. IEEE 27th Asilomar Conference on Signals, Systems and Computers, 1993.

[3] Fazel K. Performance of convolutionally coded CDMA/OFDM in a frequency-time selective fading channel and its near-far resistance. IEEE International Conference on Communications (ICC), 1994.

[4] Fettweis G, Bahai AS, Anvari K. On multi-carrier code division multiple access (MC-CDMA) modem design. IEEE Vehicular Technology Conference (VTC), 1994.

[5] Sanzi F, Slama A, Speidel J. Multicarrier code division multiplex with iterative map symbol-by-symbol estimation. IEEE Global Communication Conference (GLOBECOM), 2001.

[6] Kaiser S. OFDM code division multiplexing in fading channels. IEEE Trans Commun 2002;50:1266–73.

[7] Kaiser S, Hagenauer J. Multicarrier CDMA with iterative decoding and soft interference cancellation. IEEE Global Communication Conference (GLOBECOM), 1997.

[8] Tüchler M, Singer AC, Koetter R. Minimum mean squared error equalization using a priori information. IEEE Trans Signal Process 2002;50:673–83.

[9] Tüchler M, Koetter RCSA. Turbo equalization: principles and new results. IEEE Trans Commun 2002;50:754–67.

[10] Dejonghe A, Vandendorpe L. Turbo equalization for multilevel modulation: an efficient low-complexity scheme. IEEE International Conference on Communications (ICC) (2002).

[11] Akhter MS, Asenstorfer J, Alexander PDCRM. Performance of multicarrier CDMA with iterative detection. IEEE International Conference on Universal Personal Communications (ICUPC), 1998.

[12] Akhter MS, Asenstorfer J. Iterative detection for MC-CDMA system with base station antenna array for fading channels. IEEE Global Communication Conference (GLOBECOM), 1998.

[13] ten Brink S. Iterative decoding trajectories of parallel concatenated codes. 3rd IEEE/ITG Conference on Source and Channel Coding, 2000.

[14] ten Brink S. Design of serially concatenated codes based on iterative decoding convergence. 2nd International Symposium on Turbo Codes, 2000.

[15] ten Brink S. Convergence behavior of iteratively decoded parallel concatenated codes. IEEE Trans Commun 2001;49:1727–37.

[16] Proakis JG. Digital communication. third ed., New York: McGraw-Hill; 1995.

[17] Höher P. A statistical discrete-time model for the WSSUS multipath channel. IEEE Trans Vehicular Technol 1992;41:461–8.

[18] Hagenauer J, Offer E, Papke L. Iterative decoding of binary block and convolutional codes. IEEE Trans Inform Theory 1996;42:429–45.

[19] Bahl L, Cocke J, Jelinek F, Raviv J. Optimal decoding of linear codes for minimizing symbol error rate. IEEE Trans Inform Theory 1974;20:284–7.

[20] Choi W-J, Cheong K-W, Cioffi JM. Iterative soft interference cancellation for multiple antenna systems. IEEE Wireless Communication and Networking Conference (WCNC), 2000.

[21] ten Brink S, Speidel J, Yan R-H. Iterative demapping for QPSK modulation. IEE Electron Lett 1998;34:1459–60.

[22] ten Brink S, Speidel J, Yan R-H. Iterative demapping and decoding for multilevel modulation, IEEE Global Communication Conference (GLOBECOM), 1998.

[23] Sanzi F, Jelting S, Speidel J. A comparative study of iterative channel estimators for mobile OFDM systems. IEEE Trans Wireless Commun 2003;2:849–59.

[24] Höher P, Kaiser S, Robertson P. Two-dimensional pilot-symbol-aided channel estimation by Wiener filtering ICASSP, 1997.

[25] Höher P, Kaiser S, Robertson P. Pilot-symbol-aided channel estimation in time and frequency. International Workshop on Multi-Carrier Spread-Spectrum, 1997.

[26] Höher P, Kaiser S, Robertson P. Pilot-symbol-aided channel estimation in time and frequency, IEEE Sixth Communication Theory Mini-Conference (GLOBECOM), 1997.

[27] Sanzi F, Speidel J. An adaptive two-dimensional channel estimator for wireless OFDM with application to mobile DVB-T. IEEE Trans Broadcasting 2000;46:128–33.

Friedrich Sanzi was born in Kirchheim/Teck, Germany in 1972. He received the masters degree (Dipl.-Ing.) in 1997 and the Ph.D. degree (Dr.-Ing.) in 2003 from the Faculty of Computer Engineering, Electrical Engineering and Information Technology at the University of Stuttgart, Germany. He has been with the Institute of Telecommunications of the University of Stuttgart from November 1997 to October 2003 as a research and teaching assistant. Since November 2003 he is with Leuze electronic, Owen/Teck, Germany. His research interests include multicarrier modulation, digital signal processing and optical identification systems.